

59-34

40687

127

N95-22446

395811

Large-eddy simulation of a plane wake

By S. Ghosal AND M. Rogers¹

1. Motivation and objectives

In a previous report (Ghosal *et al.*, 1992, 1994) the theoretical development leading to the dynamic localization model (DLM) for large-eddy simulation (LES) was presented. The method has been successfully applied to isotropic turbulence (Ghosal *et al.*, 1992, 1993, 1994, Carati *et al.*, 1994 - see also the report in this volume), channel flow (Cabot, 1993 - see also the report in this volume) and the flow over a backward-facing step (Akselvoll & Moin, 1993a & b). Here we apply the model to the computation of the temporally developing plane wake. The two main objectives of this project are:

(A) Use the model to perform an LES of a time developing plane wake and compare the results with direct numerical simulation (DNS) data to see if important statistical measures can be reliably predicted. Also, to provide a relative evaluation of the several versions of the model in terms of predictive capability and cost.

(B) If the tests in (A) show that the model generates reliable predictions, then use the LES to study various aspects of the physics of turbulent wakes and mixing layers.

According to the notation introduced earlier (see the references above), we recognize four versions of DLM:

(1) Dynamic model (DM): Special case of the DLM applicable only to flows with homogeneous directions.

(2) Dynamic localization model (constrained) [DLM(+)] : A limited version of the more general DLM, explicitly prevents backscatter by enforcing a positivity requirement on the Smagorinsky coefficient.

(3) Dynamic localization model (k-equation) [DLM(k)] : Extended version of DLM that incorporates backscatter by introducing a budget equation for the sub-grid kinetic energy.

(4) Dynamic localization model (stochastic) [DLM(S)] : Alternate extension of DLM that incorporates backscatter by a stochastic term.

Tests of the DM and DLM(+) will be presented in this report. The more elaborate models DLM(k) and DLM(S) that incorporate backscatter have not yet been tested for this flow. In the next section we briefly review the two versions of the model tested. No derivations are presented here; the reader is referred to the appropriate references (Ghosal *et al.*, 1992, 1994, and references therein) for the underlying theory.

¹ NASA Ames Research Center

2. Accomplishments

2.1 Background

2.1.1 The dynamic model (DM)

In its present form, the dynamic model can be written in the following way. For homogeneous turbulence the coefficient C is constant in space (but it may be time dependent) and is given by

$$C(t) = \frac{\langle m_{ij} L_{ij} \rangle}{\langle m_{kl} m_{kl} \rangle}. \quad (1)$$

Here $L_{ij} = \widehat{u_i u_j} - \widehat{u_i} \widehat{u_j}$ is the Leonard term and $m_{ij} = \Delta^2 |\widehat{S}| \widehat{S}_{ij} - \widehat{\Delta^2} |\widehat{S}| \widehat{S}_{ij}$, where $\widehat{u_i}$ and \widehat{S}_{ij} are the filtered velocity and strain rates and the ‘hat’ denotes the ‘test filtering’ operation:

$$\widehat{f}(\mathbf{x}) = \int G(\mathbf{x}, \mathbf{y}) f(\mathbf{y}) d\mathbf{y}. \quad (2)$$

The ‘grid-level’ filter-width is Δ (usually taken to be of the order of the grid spacing) and $\widehat{\Delta}$ ($\widehat{\Delta} > \Delta$) is the ‘test-level’ filter-width. The angular brackets denote averaging over the volume of the domain.

For flows that are not completely homogeneous but have one or two homogeneous direction(s) the DM can still be applied *provided one assumes that the ‘test filtering’ operation is performed only in the homogeneous direction(s)*. Such an assumption can be justified if the grid in the inhomogeneous direction(s) is so fine that the flow is fully resolved in that direction, but in general it is not strictly valid. If one considers a flow (such as the plane wake considered in this report) that is homogeneous in the $x - z$ plane but inhomogeneous in y , then the DM can be written as

$$C(\mathbf{y}, t) = \frac{\langle m_{ij} L_{ij} \rangle_{xz}}{\langle m_{kl} m_{kl} \rangle_{xz}}. \quad (3)$$

where the angular brackets now denote averaging over the homogeneous $x - z$ planes.

A serious problem with the DM is that it can be applied only to homogeneous flows or (under additional assumptions) to flows with at least one homogeneous direction. This deficiency is removed by the DLM described next.

2.1.2 The dynamic localization model: constrained [DLM(+)]

In DLM(+) one obtains $C(\mathbf{x})$ as a function of position at each time-step by solving an integral equation

$$C(\mathbf{x}) = \left[f(\mathbf{x}) + \int \mathcal{K}(\mathbf{x}, \mathbf{y}) C(\mathbf{y}) d\mathbf{y} \right]_+ \quad (4)$$

where the suffix ‘+’ indicates the positive part and

$$f(\mathbf{x}) = \frac{1}{\alpha_{kl}(\mathbf{x}) \alpha_{kl}(\mathbf{x})} \left[\alpha_{ij}(\mathbf{x}) L_{ij}(\mathbf{x}) - \beta_{ij}(\mathbf{x}) \int L_{ij}(\mathbf{y}) G(\mathbf{y}, \mathbf{x}) d\mathbf{y} \right], \quad (5)$$

$$\mathcal{K}(\mathbf{x}, \mathbf{y}) = \frac{\mathcal{K}_A(\mathbf{x}, \mathbf{y}) + \mathcal{K}_A(\mathbf{y}, \mathbf{x}) - \mathcal{K}_S(\mathbf{x}, \mathbf{y})}{\alpha_{kl}(\mathbf{x})\alpha_{kl}(\mathbf{x})}, \quad (6)$$

$$\mathcal{K}_A(\mathbf{x}, \mathbf{y}) = \alpha_{ij}(\mathbf{x})\beta_{ij}(\mathbf{y})G(\mathbf{x}, \mathbf{y}) \quad (7)$$

and

$$\mathcal{K}_S(\mathbf{x}, \mathbf{y}) = \beta_{ij}(\mathbf{x})\beta_{ij}(\mathbf{y}) \int G(\mathbf{z}, \mathbf{x})G(\mathbf{z}, \mathbf{y}) dz. \quad (8)$$

In these expressions $G(\mathbf{x}, \mathbf{y})$ is the “test filter” $\alpha_{ij} = -2\widehat{\Delta}^2|\widehat{S}|\widehat{S}_{ij}$, $\beta_{ij} = -2\Delta^2|\overline{S}|\overline{S}_{ij}$ and L_{ij} is the Leonard term.

The principal weakness of DLM(+) (as well as the DM) is that the restriction of C to only positive values is somewhat contrived because it does not account for backscatter. However, unlike the DM, the DLM(+) is completely general and can be applied to arbitrary inhomogeneous flows.

2.1.3 The problem of the temporally developing wake

In a temporally developing wake the flow is statistically homogeneous in the streamwise (x) and spanwise (z) directions and inhomogeneous in the normal (y) direction. The governing equations are the incompressible Navier-Stokes equations with periodic boundary conditions in x and z . In the y -direction the domain is infinite and the velocity field is assumed to asymptotically approach the free-stream velocity, which can be taken as zero in a suitably chosen reference frame. This system can be considered to be an approximation to the physically more interesting spatially developing wake. If one imagines a ‘box’ being advected downstream at the ‘free-stream’ velocity, then the motion of the fluid in the imaginary box approximates a temporally developing wake. The integrated mass flux deficit

$$\mu = - \int_{-\infty}^{+\infty} \delta U(y) dy \quad (9)$$

is conserved in a temporally developing wake, as opposed to the momentum flux deficit

$$\mu_* = - \int_{-\infty}^{+\infty} (U_\infty + \delta U(y))\delta U(y) dy, \quad (10)$$

which is conserved for a spatially developing wake. Clearly, if the mean velocity deficit δU is small compared to the free stream velocity U_∞ , then $\mu_* \approx U_\infty\mu$. A suitable scale for the velocity is the initial centerplane velocity deficit $\delta U_0 = -(\delta U(0))_{t=0}$ and a suitable length scale is then $\mu/\delta U_0$. The corresponding time scale is $\mu/(\delta U_0)^2$. We will quote most of our results in these units.

2.2 Computational methods

The numerical method used is a spectral method in vorticity variables. Both the velocity and vorticity are periodic in the x and z directions and can therefore be expanded in a basis of trigonometric functions for these variables. The y -direction is somewhat more difficult to deal with since the domain is infinite in y . One

method is to choose a basis of functions that have an infinite support (such as the Jacobi polynomials coupled with a mapping to the infinite interval) for the y -direction (Spalart *et al.*, 1991). However, here we use a trick that leads to a simpler code. We take advantage of the fact that in a wake the vorticity field is much more confined in the y direction than the velocity field. One then expands the vorticity in a trigonometric series in y defined over (y_{min}, y_{max}) with periodic boundary conditions. This is permissible provided that the vorticity is narrowly confined around $y = 0$ and effectively decays to zero at the boundaries y_{min} and y_{max} . The velocity field is not so confined and cannot be represented in terms of these trigonometric functions. But once the vorticity field is determined, the correct velocity field may be obtained by adding a potential "correction" to the periodic velocity field associated with the vorticity field so as to match the boundary conditions at $y = \pm\infty$. Further details of the computational method may be found in Corral and Jimenez (1993). The method of solving the integral equation to determine the coefficient C has been described elsewhere (Ghosal *et al.*, 1992, 1994). The test filter width in these computations was taken to be twice the grid-filter width, $\hat{\Delta} = 2\Delta$, and a 'top-hat' filter was used with a Simpson's rule quadrature.

For initial conditions we take two realizations of 'turbulence over a flat plate' from DNS data generated by Spalart (1988) and 'sandwich' them to produce a wake. Physically this corresponds to a situation where two independent boundary layers exist on either side of a rigid plate and the plate is instantaneously "dissolved" without disturbing the surrounding fluid. All the parameters in the LES are chosen so as to correspond to the "unforced wake" case of Moser and Rogers (1994) mentioned above.

The LES reported here was performed on a grid of size $Nx = 64$, $Ny = 48$, and $Nz = 16$. Therefore, all DNS data must first be 'filtered' to the same resolution as the LES. This is done by truncating the DNS data in Fourier space to the same number of modes retained in the LES. This filtering procedure is applied to the initial conditions as well as to all DNS data with which we wish to compare our LES results. The 'filtered DNS' represents the theoretical best that can be achieved by any LES. The LES with DM took about 11 minutes of CPU time. For the DLM(+) the CPU time depended on the level of convergence required for the solution of the integral equation. We measured the degree of convergence by the rms error in satisfying the integral equation normalized by the maximum value of $\langle C \rangle_{zz}$. When it was required that the error as defined above should not exceed 10^{-4} , the DLM(+) used about 18 minutes of CPU time. To test if this level of convergence was adequate, the simulation was rerun with the convergence criterion set at 10^{-9} . There were no observable differences in any of the computed statistical measures. For comparison, the high resolution DNS of Moser and Rogers of the same flow over the same time interval cost about 200 CPU hours. All computations were performed on a CRAY C90.

2.3 Results

The gross features of the wake are characterized by the maximum wake deficit δU_m of the mean velocity profile and the 'half-width' b of the wake. The half-width

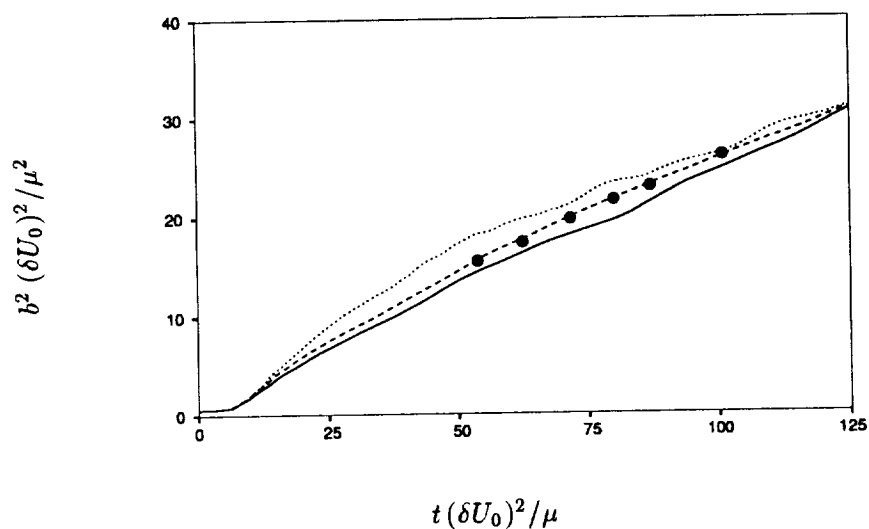


FIGURE 1. The square of the wake-width as a function of time using DLM(+) —; DM - - -; No model ·····; filtered DNS •

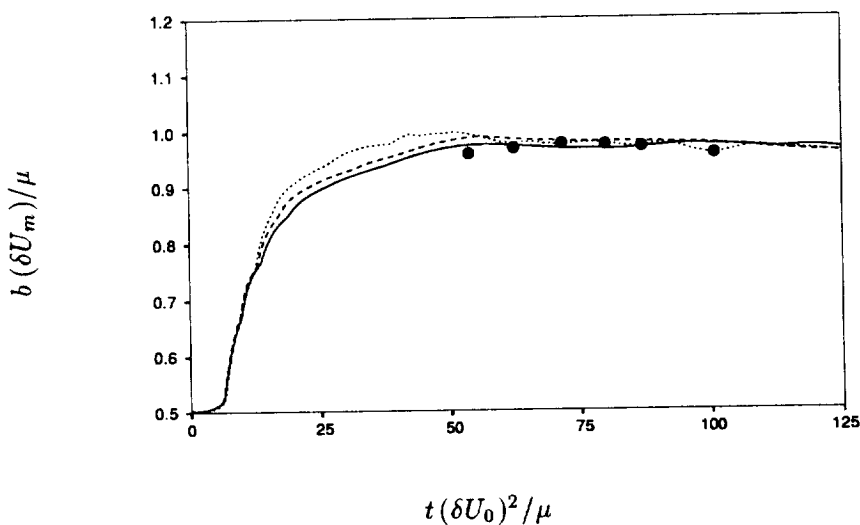


FIGURE 2. The product of the wake-width and the maximum velocity deficit as a function of time using DLM(+) —; DM - - -; No model ·····; filtered DNS •

is defined here as the distance between the two points at which the mean velocity deficit is half its maximum value. Fig. 1 shows b^2 plotted as a function of the time t for the LES, filtered DNS, and LES with the subgrid model turned off. The prediction of the DM is closest to the filtered DNS. The width grows as $b \sim \sqrt{t}$

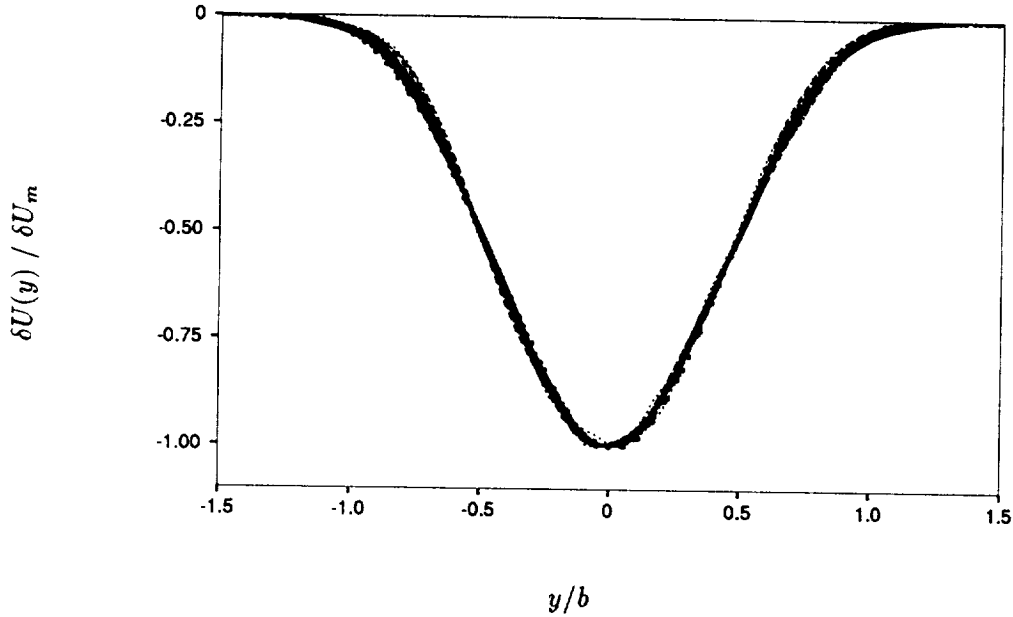


FIGURE 3. The mean wake velocity deficit in self-similar coordinates using DLM(+) —; DM - - -; No model ·····; filtered DNS ●

in the self-similar region ($t(\delta U_0)^2/\mu \approx 50 - 100$) as expected. Fig. 2 shows the product $b(\delta U_m)$ as a function of t . In all cases this quantity exhibits a plateau during the self-similar period. Note that the Reynolds number $Re_b = b\delta U_m/\nu = 2000b\delta U_m/\mu \approx 2000$ in the self-similar period.

Fig. 3 shows the mean velocity profile plotted in self-similar coordinates $\delta U_* = \delta U/\delta U_m$ and $y_* = y/b$ for $t(\delta U_0)^2/\mu \approx 50 - 100$. In all cases very good self-similar collapse is observed (even with the subgrid model turned off!). Thus, the mean velocity profile is quite insensitive to the subgrid model.

Figs. 4 (A), (B), (C), and (D) show the second-order velocity statistics $\langle u^2 \rangle$, $\langle v^2 \rangle$, $\langle w^2 \rangle$, and $\langle uv \rangle$ respectively. Here u , v , and w are the velocities in the x , y , and z directions, respectively, with the mean velocity subtracted out. The angular brackets denote averaging over $x - z$ planes. In all cases it is observed that both the DM and DLM(+) predict the second-order statistics very well. The quality of the predictions deteriorates significantly if the model is turned off (except for $\langle uv \rangle$). The better agreement for the $\langle uv \rangle$ profile is to be expected since it is directly related to the mean velocity profile $\delta U(y)$ through the x -component of the momentum equation and we have already seen that $\delta U(y)$ is insensitive to the subgrid model.

Figs. 5 (A), (B), (C), and (D) show the second-order vorticity statistics $\langle \omega_x^2 \rangle$, $\langle \omega_y^2 \rangle$, $\langle \omega_z^2 \rangle$, and $\langle \omega_x \omega_y \rangle$ respectively. Here ω_x , ω_y , and ω_z are the vorticities in the x , y , and z directions, respectively, with the mean vorticity subtracted out. The angular brackets denote averaging over $x - z$ planes. The agreement of the DM as well as the DLM(+) predictions with the filtered DNS is seen to be very good. When the

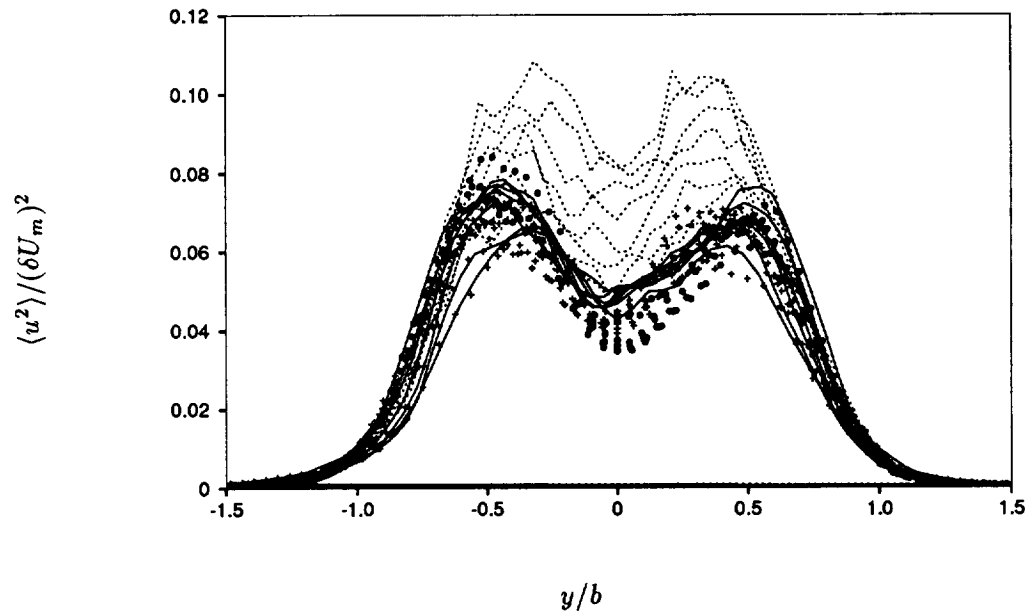


FIGURE 4A. The mean streamwise intensity of turbulence in self-similar coordinates using DLM(+) +; DM —; No model ·····; filtered DNS •

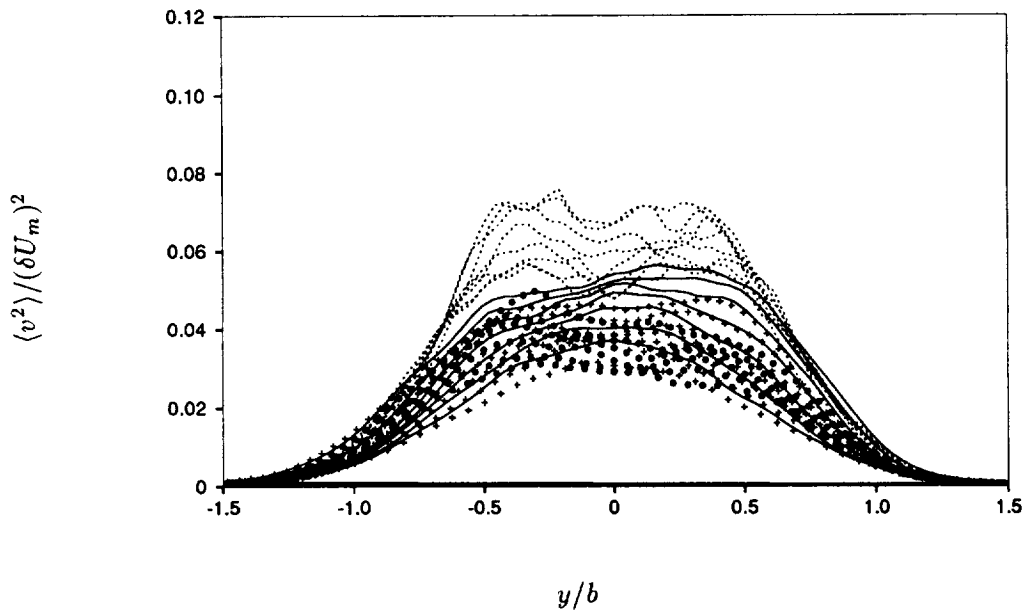


FIGURE 4B. The mean cross-stream intensity of turbulence in self-similar coordinates using DLM(+) +; DM —; No model ·····; filtered DNS •

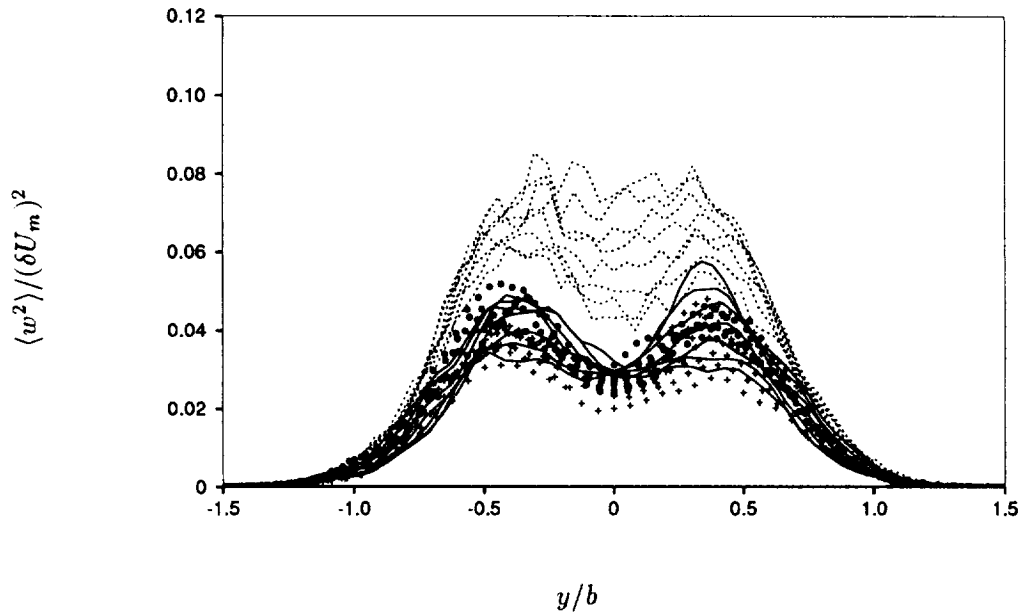


FIGURE 4C. The mean spanwise intensity of turbulence in self-similar coordinates using DLM(+) +; DM —; No model ·····; filtered DNS •

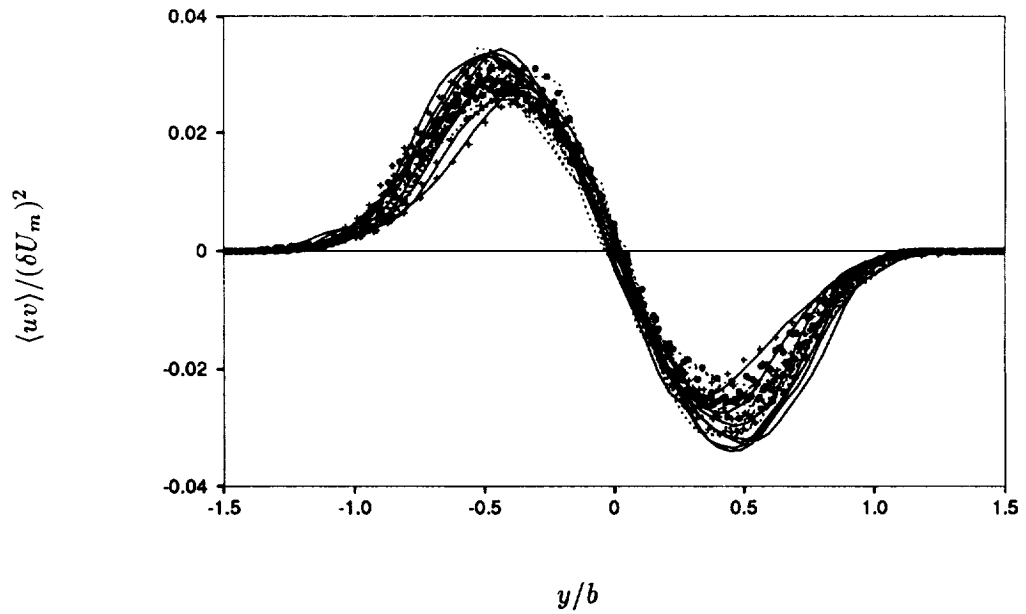


FIGURE 4D. The mean turbulent stress uv in self-similar coordinates using DLM(+) +; DM —; No model ·····; filtered DNS •

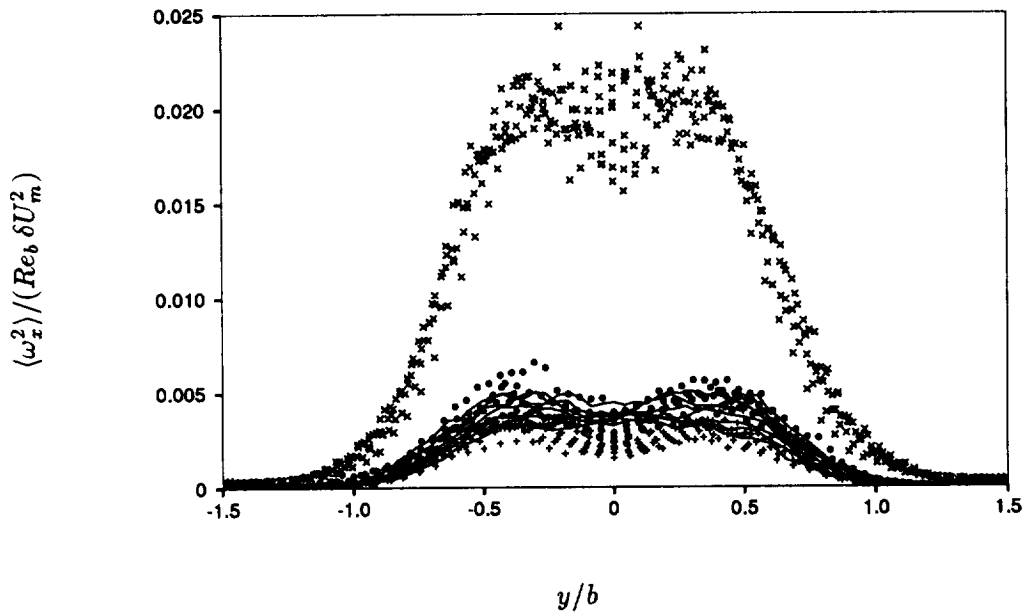


FIGURE 5A. The mean intensity of streamwise vorticity in self-similar coordinates using DLM(+) +; DM —; No model ×; filtered DNS •

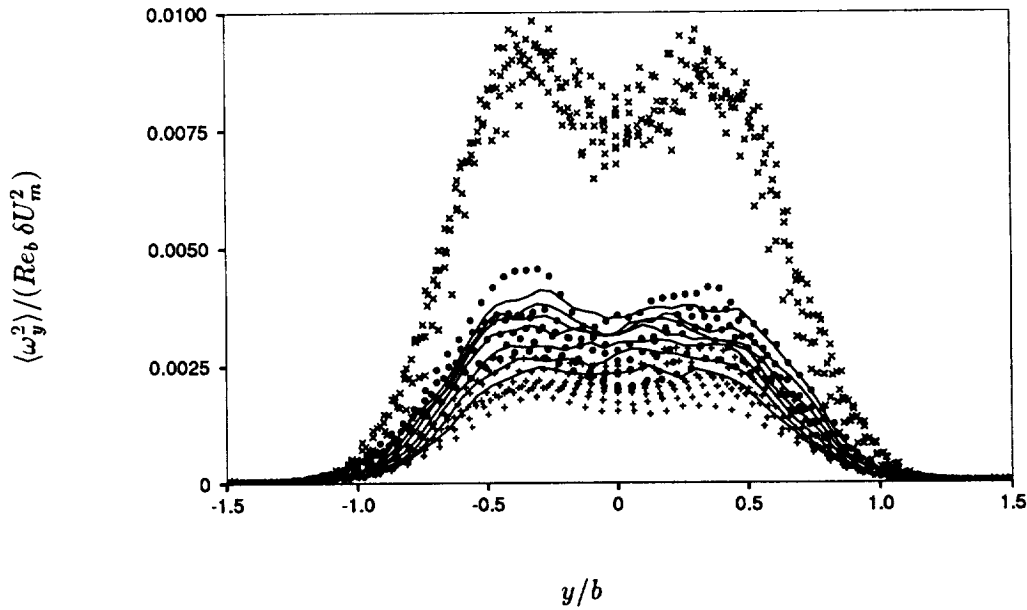


FIGURE 5B. The mean cross-stream intensity of vorticity in self-similar coordinates using DLM(+) +; DM —; No model ×; filtered DNS •

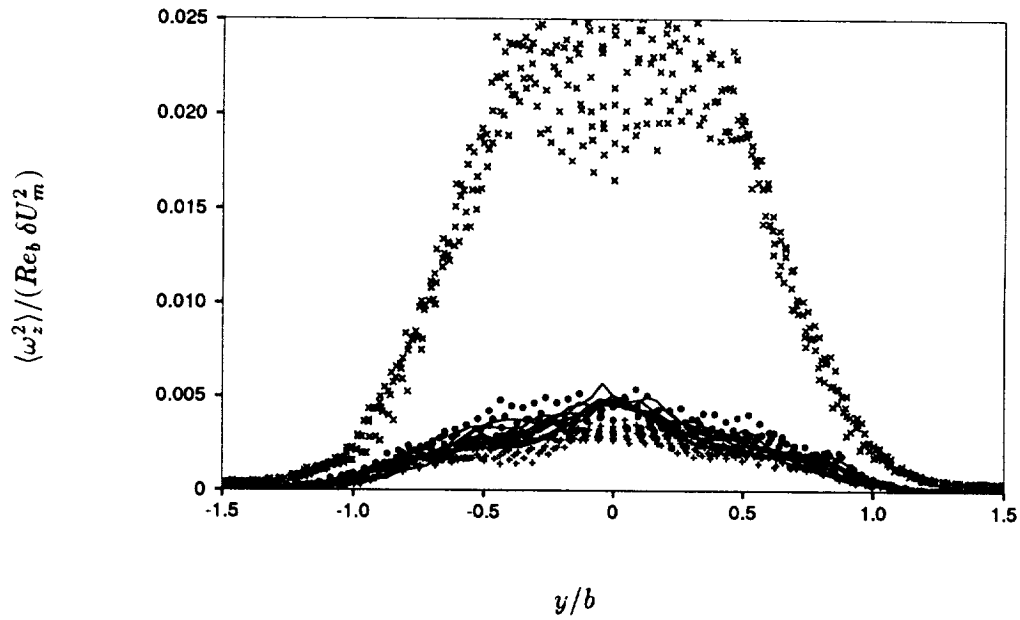


FIGURE 5C. The mean spanwise intensity of vorticity in self-similar coordinates using DLM(+) +; DM —; No model \times ; filtered DNS \bullet

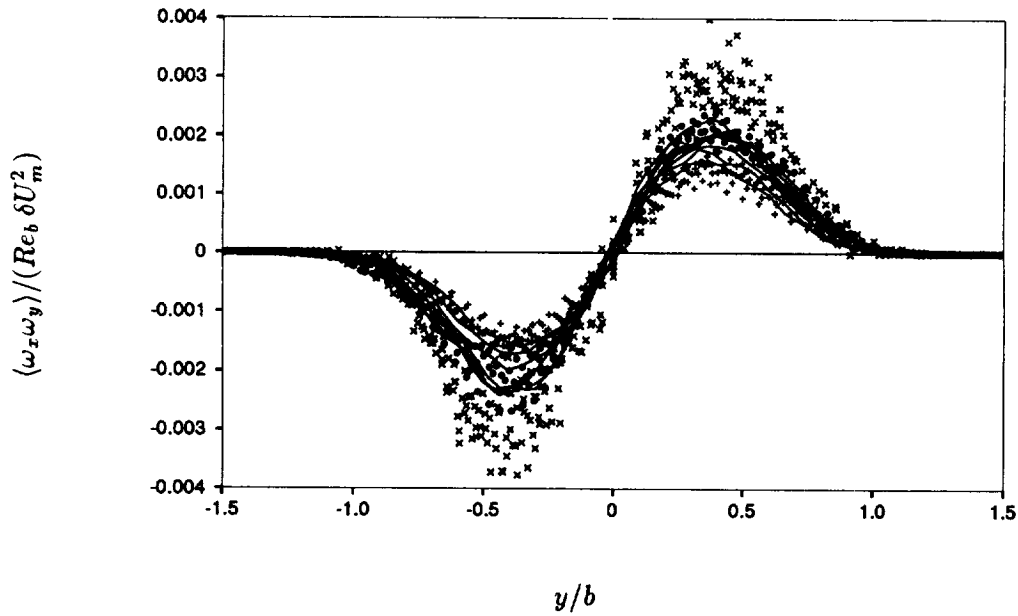


FIGURE 5D. The mean vorticity product $\omega_x \omega_y$ in self-similar coordinates using DLM(+) +; DM —; No model \times ; filtered DNS \bullet

model is turned off the agreement with the filtered DNS is seen to be very poor. The magnitudes of the enstrophy components are about four times the corresponding filtered DNS levels. Here one might ask if it is reasonable or useful to use an LES to predict vorticity statistics since it is known that small scales not resolved by LES are the primary contributors to enstrophy. Indeed, $\langle \omega_x^2 \rangle$, $\langle \omega_y^2 \rangle$, and $\langle \omega_z^2 \rangle$ for the filtered DNS are about a fifth of their levels in the unfiltered DNS. However, good prediction of vorticity statistics is important because these statistics are a sensitive measure of the scales close to the threshold of resolution of the LES. The fact that even vorticity statistics are captured by the LES suggests that all of the resolved scales and not just the lowest wavenumber modes are faithfully represented in the simulation. Thus, we use vorticity statistics as a “quality indicator” of the LES rather than as a quantity of practical importance to the user.

In Figs. 4 and 5 it is apparent that the self-similar collapse is not perfect but that there is a systematic variation between the curves at different times in the simulation, even when scaled in self-similar variables. This is the case not only for the LES, but also for the filtered DNS. This is an artifact of the filtering procedure itself and can be understood in the following way. The flow evolves self-similarly at constant Reynolds number $Re_b = b(\delta U_m)/\nu$ (see Fig. 2) in the self-similar region but the length scales increase in time. Thus, as the flow evolves, the energy spectrum shifts to the left without changing form. Since the grid size is held fixed, this implies that more and more of the energy becomes ‘resolved’ as the spectrum shifts to lower wavenumbers past $\bar{k} = 2\pi/\Delta$. Therefore the resolved part of the second-order statistics increases with time. This is precisely what is observed in the filtered DNS and LES data and is responsible for the systematic increasing trend during the self-similar period.

In addition to obtaining quantitative predictions, one also hopes to gain some qualitative understanding of the large-scale flow structures from an LES. Thus, it is of interest to see if the model is able to generate structures that look realistic. As an example a typical contour plot of the v -velocity is presented in Fig. 6 over an $x-y$ plane. It is seen that Fig. 6(C) (LES with model) bears an overall resemblance to Fig. 6(B) (filtered DNS) in the sense that it has a similar number of ‘eddies’ of approximately similar size and shape. However, Fig. 6(D) (LES without model) looks qualitatively different from Fig. 6(B) in the sense that it has a profusion of poorly resolved small-scale structures. A similar statement can be made about the other flow variables. The times at which the contours are shown in Fig. 6 for the DNS and LES do not correspond exactly, but they are close, varying from $t(\delta U_0)^2/\mu \approx 62.4$ to 66.3, and are in the developed region (see Fig. 1).

It may appear that even though the no-model case (Fig. 6(D)) has far too many small-scale fluctuations compared to the filtered DNS (Fig. 6(B)), it does resemble somewhat the full DNS of Fig. 6(A). That this is not the case becomes clear on examination of the energy spectrum. Fig. 7 shows the one-dimensional spectrum

$$q^2(k_x) = \sum_{k_z} (|\tilde{u}(k_x, k_z)|^2 + |\tilde{v}(k_x, k_z)|^2 + |\tilde{w}(k_x, k_z)|^2) \quad (11)$$

at the plane $y = 0$ for the same fields whose v -contour plots are shown in Fig. 6.

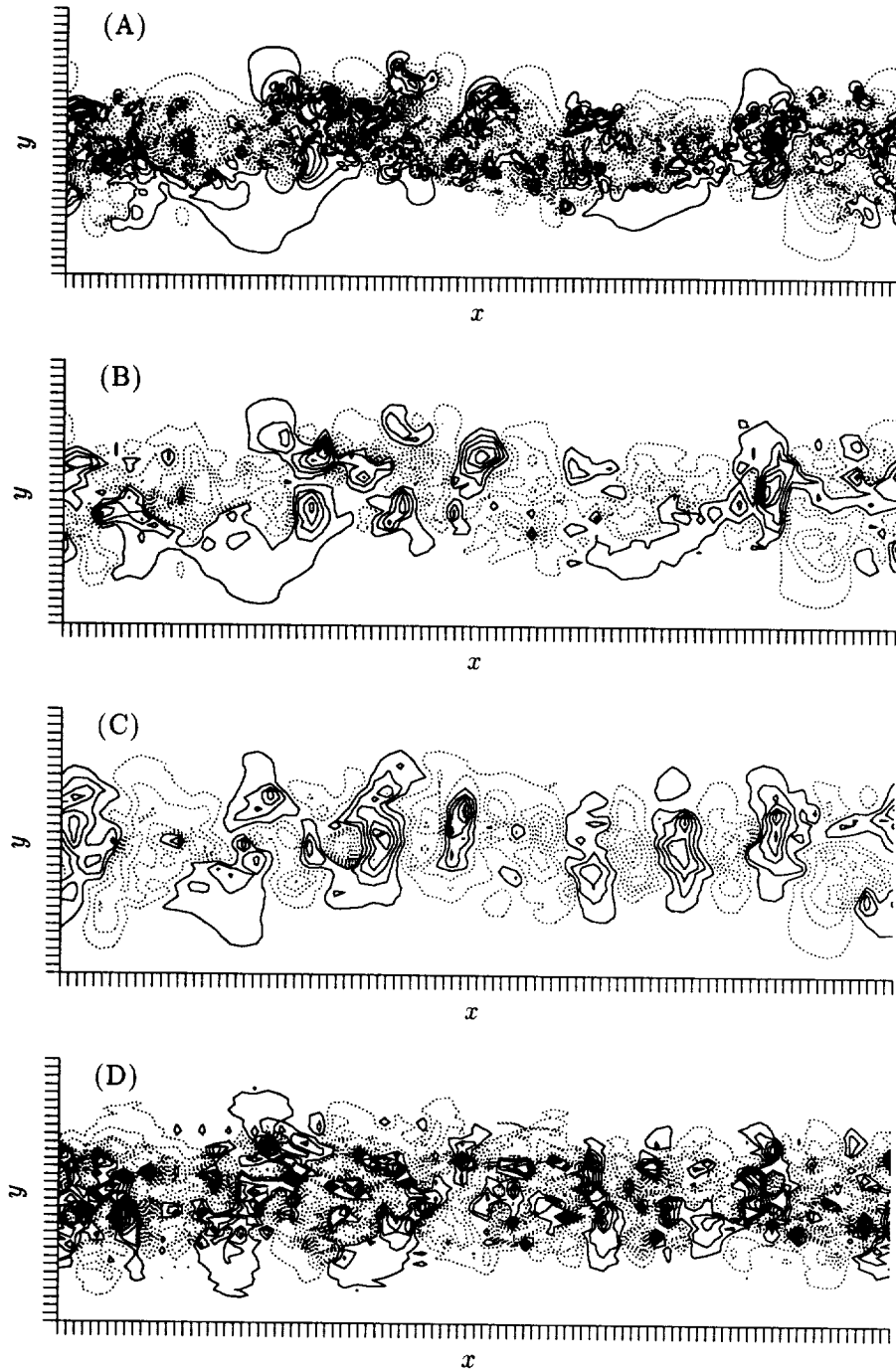


FIGURE 6. A typical iso-velocity contour plot for component v in the $x - y$ plane for (A) DNS (B) Filtered DNS (C), DLM(+) and (D) No model.

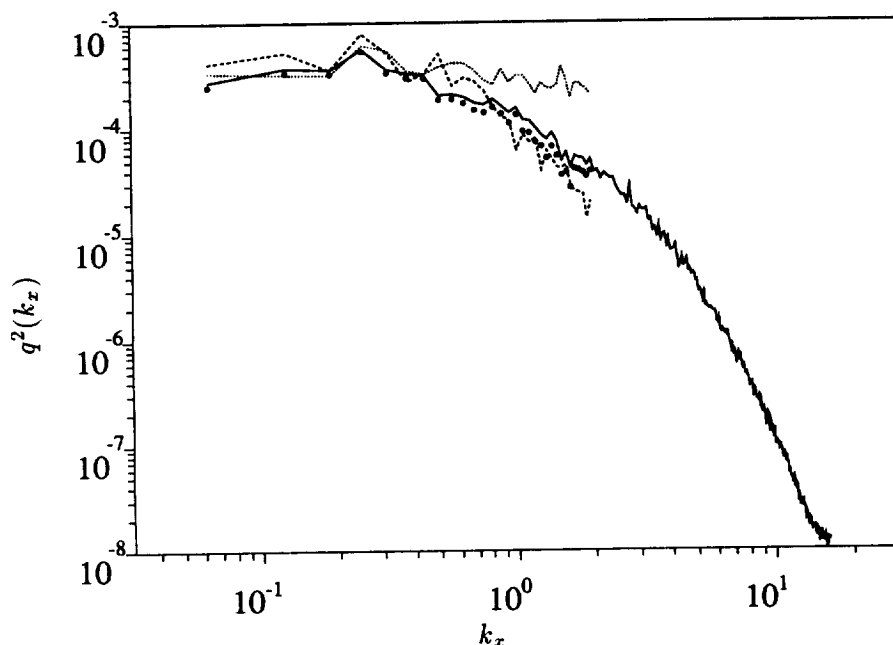


FIGURE 7. The ' q^2 -spectrum' (see text) for LES using DLM(+) - - -; using no model ·····; filtered DNS •; DNS —.

Here ' \sim ' denotes Fourier-transform in the $x-z$ plane. The filtered DNS is very close to, but slightly below (on account of filtering in the y -direction), the full DNS, up to the maximum k_x represented in the LES. The LES matches the filtered DNS closely. However, for the no-model case, energy piles up at the high wavenumbers because of the lack of a dissipation mechanism, and this results in a 'flat' rather than decaying energy spectrum. The small-scale fluctuations seen in Fig. 6(D) are a manifestation of this unphysical 'pile-up' of energy and have no relation to the true fine structure seen in the highly resolved DNS of Fig. 6(A). Indeed, it is quite impossible to reproduce the fine structure of the DNS with the vastly reduced number of modes in an LES, and the 'filtered' DNS is the ideal limit one can hope to achieve.

In summary, mean velocity profiles plotted in self-similar coordinates are very insensitive to the choice of subgrid models. The prediction of the self-similar growth of the wake width is improved by the subgrid model, but the results with no model are nevertheless tolerable. Second-order velocity and vorticity statistics are predicted very well by both the DM and DLM(+), but the predictions of these statistics without the model are very poor. The flow structures in the LES have a strong visual resemblance to those of the corresponding filtered DNS, but this is not the case if the LES is performed with no subgrid model. The LES represents a very significant saving in CPU time over the corresponding DNS. The results presented here suggest that LES can provide accurate predictions when information related to small-scale structures is not required.

3. Future plans

In generating the results presented in this report, the “test filter” was implemented only in the x and z directions. This was done as a first step because filtering only in the homogeneous directions is easiest to implement in the code. However, there are some serious difficulties associated with this. In situations where the grid spacings in all three directions are not the same, there is no unique way of defining the “grid-filter width” Δ . Some possible choices are

$$(A) \Delta = (\Delta_x \Delta_y \Delta_z)^{1/3}$$

$$(B) \Delta = (\Delta_x^2 + \Delta_y^2 + \Delta_z^2)^{1/2}$$

$$(C) \Delta = \max [\Delta_x, \Delta_y, \Delta_z]$$

$$(D) \Delta = (\Delta_x \Delta_z)^{1/2}.$$

The choice (D) may be thought of as a natural modification of (A) when $\Delta_y \ll \Delta_x, \Delta_z$. In this case (A) would give an unreasonably small length scale.

Now, if the filtering is done in all three directions, then $\hat{\Delta}_x = 2\Delta_x$, $\hat{\Delta}_y = 2\Delta_y$, and $\hat{\Delta}_z = 2\Delta_z$ so that all the possible choices (A), (B), (C), and (D) give the same value for the filter-width ratio $\hat{\Delta}/\Delta = 2$. It is easily shown that only the combination $C\Delta^2$ is computed in the dynamic model and that the grid and test filter-widths enter only as the ratio $\hat{\Delta}/\Delta$. Thus when the model is properly implemented with a 3D-filter, it is unaffected by the choice of filter-width definition. In fact, any filter width $\Delta = f(\Delta_x, \Delta_y, \Delta_z)$ where f is a homogeneous function (i.e. $f(a\Delta_x, b\Delta_y, c\Delta_z) = abc f(\Delta_x, \Delta_y, \Delta_z)$) will yield the same filter-width ratio. This is no longer true if the filtering is only done in $x - z$ planes as in the current simulations. In this case $\hat{\Delta}_x = 2\Delta_x$, $\hat{\Delta}_y = \Delta_y$, and $\hat{\Delta}_z = 2\Delta_z$, so that (C) and (D) give $\hat{\Delta}/\Delta = 2$. (A) gives $\hat{\Delta}/\Delta = 2^{2/3}$, and (B) gives a result that depends on the aspect ratio of the grid. In the simulations presented here we have chosen $\hat{\Delta}/\Delta = 2$, but the results change significantly if an alternate value for this ratio is used. These results should therefore be regarded as preliminary, and more careful tests using full 3D filtering need to be done before they can be considered reliable.

We would like to test two other versions of the dynamic localization model viz. DLM(k) and DLM(S). The first one accounts for backscatter by means of a budget equation for the subgrid kinetic energy (Ghosal *et al.*, 1992, 1994) while the second regards backscatter as a stochastic forcing. Apart from being able to represent backscatter (which may or may not be a significant effect), the DLM(k) has the additional advantage that it allows one to compute the full subgrid-stress tensor instead of simply the deviatoric part. This makes it possible to determine the resolved pressure, a quantity that cannot be determined if only the deviatoric part of the stress is known.

Both DNS and experiments on plane wakes show a range of growth rates that seem to be sensitive to initial conditions (Moser and Rogers, 1994). It has been proposed that this could be due to the existence of non-unique self-similar states, any one of which can be selected in a given realization depending on the initial conditions (George, 1989). In order to investigate such possible dependence on initial conditions, Moser and Rogers (1994) amplified the 2D components of the initial velocity field in their simulation. It has been found that it is possible to

significantly alter the growth rate by such “2D forcing”. We would like to check if LES is able to predict correctly the growth rates in such forced wakes. If it does, then LES can be used as a research tool to test whether alternate self-similar states are indeed sustained. This requires long-time simulations that are prohibitively expensive using current DNS.

We would like to thank Dr. Parviz Moin for his critical comments on an earlier version of this manuscript.

REFERENCES

- AKSELVOLL, K. & MOIN, P. 1993a Large-eddy simulation of a backward facing step flow. *2nd international symposium on engineering turbulence modeling and measurements*, Florence, Italy.
- AKSELVOLL, K. & MOIN, P. 1993b Application of the dynamic localization model to large-eddy simulation of turbulent flow over a backward facing step. *ASME Fluids engineering conference*, Washington D. C.
- CABOT, W. 1993 Dynamic localization and second-order subgrid-scale models in large-eddy simulations of channel flow. *Annual Research Briefs-1993* Center for Turbulence Research, Stanford Univ./NASA Ames, 129-144.
- CARATI, D., GHOSAL, S. & MOIN, P. 1994 On the representation of backscatter in dynamic localization models. *Phys. of Fluids* (submitted).
- CORRAL, R. & JIMENEZ, J. 1993 Fourier/Chebyshev methods for the incompressible Navier-Stokes equations in infinite domains. *J. Comp. Phys.* (to appear).
- GEORGE W. K. 1989 The self preservation of turbulent flows and its relation to initial conditions and coherent structure. *Advances in Turbulence*, Ed. W. K. George & R. Arndt (Hemisphere, New York).
- GHOSAL, S., LUND, T. S. & MOIN, P. 1992 A local dynamic model for large-eddy simulation. *Annual Research Briefs-1992* Center for Turbulence Research, Stanford Univ./NASA Ames, 3-25.
- GHOSAL S. 1993 On the large-eddy simulation of turbulent flows in complex geometry. *Annual Research Briefs-1992* Center for Turbulence Research, Stanford Univ./NASA Ames, 111-128.
- GHOSAL, S., LUND, T. S., MOIN, P. & AKSELVOLL, K. 1994 A dynamic localization model for large-eddy simulation of turbulent flows. *J. Fluid Mech.* (to appear).
- MOSER, R. D. & ROGERS, M. M. 1994 Direct simulation of a self-similar plane wake. *NASA Tech. Mem.* **108815**.
- SPALART, P. R., MOSER, R. D. & ROGERS, M. M. 1991 Spectral methods for the Navier-Stokes equations with one infinite and two periodic directions. *J. Comp. Phys.* **96**, 297-324.
- SPALART, P. R. 1988 Direct simulation of a turbulent boundary layer up to $Re_\theta = 1410$. *J. Fluid Mech.* **187**, 61-98.

